The Limits of Lamellae-Forming PS-*b*-PMMA Block Copolymers for Lithography

Lei Wan,[*,†] Ricardo Ruiz,[†] He Gao,[†] Kanaiyalal C. Patel,[†] and Thomas R. Albrecht[†]

[†]HGST, A Western Digital Company, San Jose Research Center, 3403 Yerba Buena Road, San Jose, California 95135, United States

Jian Yin,[‡] Jihoon Kim,[‡] Yi Cao,[‡] and Guanyang Lin[‡]

[‡]EMD Performance Materials Corp., 70 Meister Avenue, Somerville, New Jersey 08876, United States

ABSTRACT We explore the lithographic limits of lamellae-forming PS-*b*-PMMA block copolymers by performing directed self-assembly and pattern transfer on a range of PS-*b*-PMMA materials having a full pitch from 27 to 18.5 nm. While directed self-assembly on chemical contrast patterns was successful with all the materials used in this study, clean removal of PMMA domains and subsequent pattern transfer could only be sustained down to 22 nm full pitch. We attribute this limitation to the width of the interface, which may represent more than half of the domain width for materials with a critical dimension below 10 nm. With the limit of pattern transfer for PS-*b*-PMMA set at ∼11 nm, we propose an integration scheme suitable for bit patterned media for densities above 1.6 Tdot/in^2, which require features below this limit. Directed self-assembly was carried out on chemical contrast patterns made by a rotary e-beam lithography system, and pattern transfer was carried out to demonstrate fabrication of large area (up to 25 mm-wide annular band of circular tracks) nanoimprint templates for bit patterned media. We also demonstrate compatibility with hard disk drive architecture by fabricating patterns with skewed radial lines with constant angular pitch and with servo patterns that are needed in hard disk drives to generate a radial positional error signal (PES).

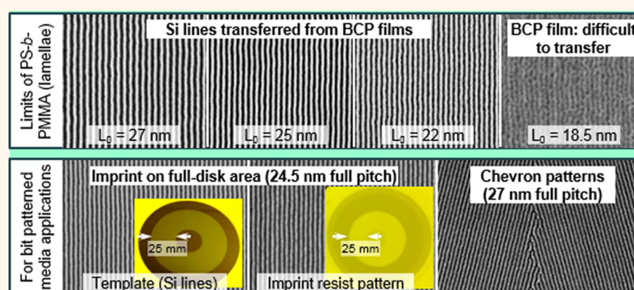

KEYWORDS: block copolymer lithography · pattern transfer · bit-patterned media · rotary e-beam lithography · nanoimprint template fabrication · PS-*b*-PMMA · lamellae

Block copolymer (BCP) directed self-assembly (DSA) is one of the most promising options for nanofabrication beyond the limits of conventional optical lithography. DSA is currently considered for future nodes of the ITRS roadmap,[1] and it is perhaps the only viable way to define the dense features needed in the fabrication of templates for magnetic bit patterned media (BPM).[2−6]

Poly(styrene-*b*-methyl methacrylate) (PS-*b*-PMMA) is perhaps the most mature and well-studied block copolymer material, making it the most likely BCP for first insertion into manufacturing. There already exists a wealth of creative methods to generate chemoepitaxy[3,7−12] or graphoepitaxy[13−17] guiding patterns as well as a large family of surface modification polymer mats and brushes[18−20] for DSA of PS-*b*-PMMA. Additionally, both PS and PMMA display almost equal surface energies, making the formation of perpendicularly oriented domains with respect to the top free interface of a thin film particularly straightforward, provided the bottom interface has neutral wetting properties. However, PS-*b*-PMMA suffers from a relatively low Flory−Huggins interaction parameter χ, which limits both the smallest achievable pitch and the width of the domain interface.[21] While phase separation in lamellae-forming PS-*b*-PMMA has been demonstrated at dimensions as low as 17.5 nm full pitch,[22] pattern transfer will most likely be limited to slightly larger dimensions because of the interface width.

BPM requires the formation of rectangular arrays of features with densities well

* Address correspondence to lei.wan@hgst.com.

Received for review April 30, 2015 and accepted June 5, 2015.

Published online June 05, 2015
10.1021/acsnano.5b02613

© 2015 American Chemical Society

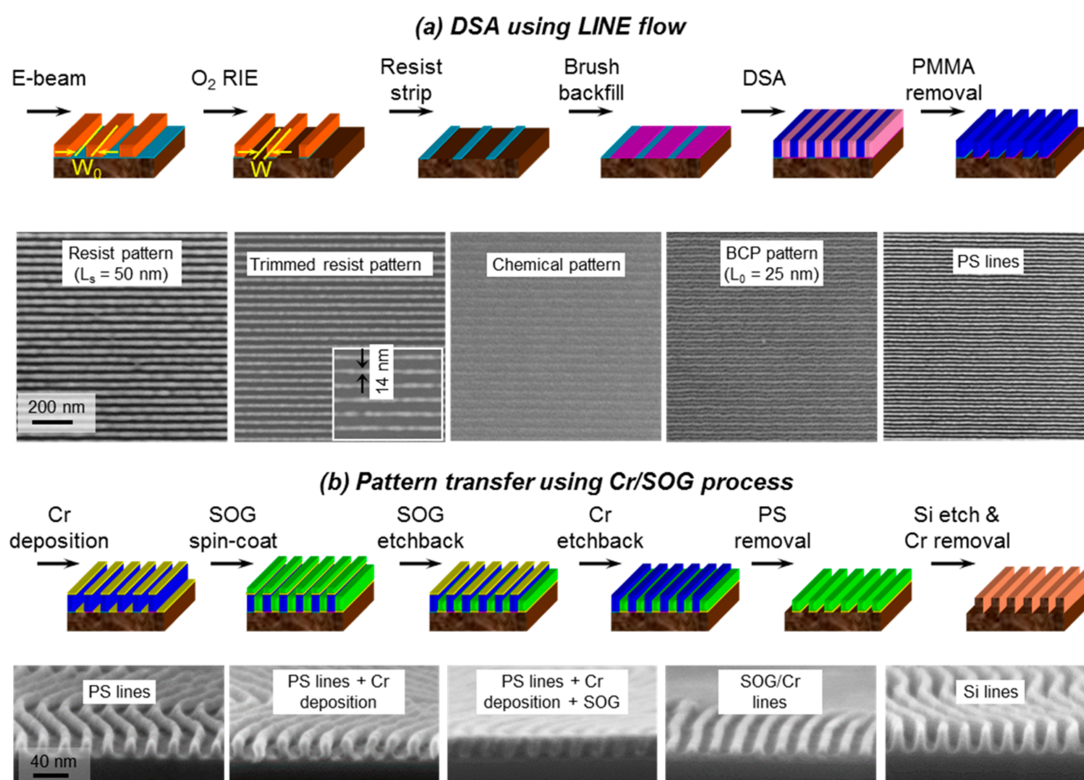

Figure 1. Schematic representation of BCP lithography. (a) DSA on chemical patterns using LINE flow: procedures are shown on top and top-down SEM images of representative steps are shown in the bottom row. (b) Pattern transfer from BCP films using Cr/SOG process: procedures are shown on top and crossectional SEM images of representative steps are shown in the bottom row.

above 1 tera dots per square inch (Tdot/in^2) with a bit aspect ratio (BAR) in the range of 1 < BAR < 2. Such rectangular patterns can be formed by intersecting two orthogonal arrays of lines (*i.e.*, radial and circumferential) originating from PS-*b*-PMMA.[23−25] However, at areal densities above 1.6 Tdot/in^2, at least one of the two arrays of stripes should have a pitch below 20 nm. Given that no other block copolymer is as mature from a processing point of view, we have previously proposed a method using self-aligned double patterning (SADP) combined with DSA of PS-*b*-PMMA as a near-term solution to reach below 20 nm full pitch.[26] SADP, however, is a complex and expensive process with difficult-to-control tolerances. Finding the limits of pattern transfer with PS-*b*-PMMA is therefore beneficial to determine the feature size beyond which the addition of complex processes such as SADP may be required.

Integrating BCP DSA into the fabrication of templates for BPM demands consideration of additional design aspects exclusive to the architecture of rotating disk magnetic recording such as servo patterns and data zoning, which require slight distortions to the natural periodicity of the BCPs. In this manuscript we first test the limits of lamellae-forming block copolymers to form robust masks for pattern transfer in the range of 13 to 9 nm critical dimensions (CDs), finding the limit at around 11 nm. With this limitation in mind, we then propose a method for the fabrication of submaster templates for BPM based on DSA of PS-*b*-PMMA BCP. This method integrates necessary pattern elements for servo patterns into the submaster template that contains the circumferential track lines, while the submaster template that contains the data radial lines is divided into zones with corresponding pitch-compressing and -stretching such that a constant angular period is maintained within each zone. The array of radial "spokes" is also slightly curved to match the skew angle of a recording head in a hard disk drive (HDD). Lastly, we demonstrate that this integration scheme can support pattern areas large enough for a full disk by fabricating a full disk-size template suitable for nanoimprinting.

RESULTS AND DISCUSSION

Figure 1 illustrates the processes we used to fabricate nanoimprint templates using BCP lithography, including DSA of BCP thin films on lithographically defined chemical patterns using the Liu−Nealy (LINE) flow,[27] and subsequent pattern transfer from the BCP patterns to the underlying substrate using a dry lift-off method incorporating the deposition of Cr and spin-on glass (SOG). The DSA procedures are shown in Figure 1a by a series of diagrams and SEM images. Chemical patterns are created on silicon substrates by first depositing a thin layer of cross-linked polystyrene (XPS) mat with ∼7−8 nm thickness. Then a layer of ZEP 520A e-beam resist is applied and patterned with rotary stage e-beam lithography. The ZEP resist

patterns are then exposed to O_2 plasma for an extended time to remove XPS mat in unprotected regions and to trim the patterned lines of XPS mat to a width w comparable to the width of the PS lamellae. After thoroughly stripping the resist, a hydroxyl-terminated poly(styrene-*r*-methyl methacrylate) (PS-*r*-PMMA-OH) brush is grafted in the regions between XPS stripes. The resulting chemical patterns have a period L_s equal to nL_0, where n is an integer. Thin films of a symmetric PS-*b*-PMMA are spin-coated on the chemical patterns. The samples are annealed at ~250 °C for a minimum of 5 min. PMMA blocks are selectively removed by O_2 reactive ion etching (RIE), leaving PS lines on the substrate. The SEM images show the steps of this process for one DSA example, where L_0 ~ 25 nm and $L_s = 2L_0$. In order to evaluate the quality of the PS lines as lithographic masks, a robust pattern transfer method is needed that can achieve good image transfer even when the remaining PS lines are only a few nm thick. We have observed that additive reverse-tone processes based on deposition of an inorganic mask consistently outperform subtractive processes based on direct etching with the PS lines serving directly as the etch mask. Here we employ a type of "dry lift-off" method that utilizes a bilayer formed by Cr followed by a planarizing spin-on glass (SOG) as shown in Figure 1b. A thin layer of Cr is deposited on the PS lines and exposed substrate regions by e-beam evaporation. Then a layer of SOG is applied by spin-coating. The SOG planarizes the surface by filling the trenches between the PS lines and leaving a thinner film on top of the PS lines. An etch-back process, using CF_4/O_2 RIE, is then carried out to remove the topmost portion of SOG in order to reveal the Cr layer above the PS lines. Cl_2/O_2 and O_2 RIE are subsequently used to etch the exposed Cr layer on top of the PS lines and the PS lines, respectively. Meanwhile, the Cr lines in the trenches are protected by the remaining SOG, and these Cr lines can serve as a mask for Si substrate etching. The cross-sectional SEM images show a sequence of steps for one sample, on which a 25 nm PS-*b*-PMMA fingerprint pattern was transferred to the silicon substrate.

When considering lithographic applications, we are interested not only in the smallest achievable dimension at which PS-*b*-PMMA can phase separate, but also on the smallest dimension at which a mask for pattern transfer can be well-defined. In order to find this mask resolution limit, we tested a few symmetric PS-*b*-PMMA BCPs with progressively lower molecular weights with periodicities ranging from 27 to 18.5 nm. In BCPs, the segregation strength is given by the product χN where χ is the Flory–Huggins interaction parameter and N is the degree of polymerization.[21] According to mean field theory, the product χN needs to be higher than 10.5 for phase separation to occur.[28] The periodicity, or pitch, of the pattern is given by $L_0 = \alpha\chi^{1/6}N^{\delta}$, where α is the statistical segment length and the exponent $\delta = 2/3$ in the strong segregation regime.[29] Finally, the interfacial width between the two domains, Δ, is given by $\Delta = 2\alpha/(6\chi)^{1/2}[1 + \ln 2(1/\chi N_A + 1/\chi N_B)]$.[30,31] For PS-*b*-PMMA, $\chi = 0.028 + 3.9/T$, where T is absolute temperature. Δ has been reported to be around 5 nm.[22,32] The smallest pitch demonstrations of self-assembly with symmetric PS-*b*-PMMA are in the range of 17.5[22] to 19 nm[33] pitch in agreement with mean field theory predictions even within the strong segregation regime with $\delta = 2/3$ assuming annealing temperatures in the range of 170–250 °C. In contrast, previously published pattern transfer demonstrations have been limited to pitch greater than 24–28 nm.[34–37] Figure 2a–c show a series of Si line patterns made from PS-*b*-PMMA having full pitch of 27, 25, and 22 nm, respectively. These line patterns were first formed using DSA with 2X density multiplication, and transferred to Si using the Cr/SOG process outlined above. The values of 3σ of the line width roughness ($3\sigma_w$), line position roughness ($3\sigma_p$), and line edge roughness ($3\sigma_e$) of the silicon lines are shown in a graph in Figure 2d. With decreasing pitch, the roughness slightly increases, but all have $3\sigma < 3$ nm. At the minimum L_0 of 22 nm, the increased roughness may have several origins. First, the phase separation of the BCP is reaching the weak segregation limit; *e.g.*, the χN

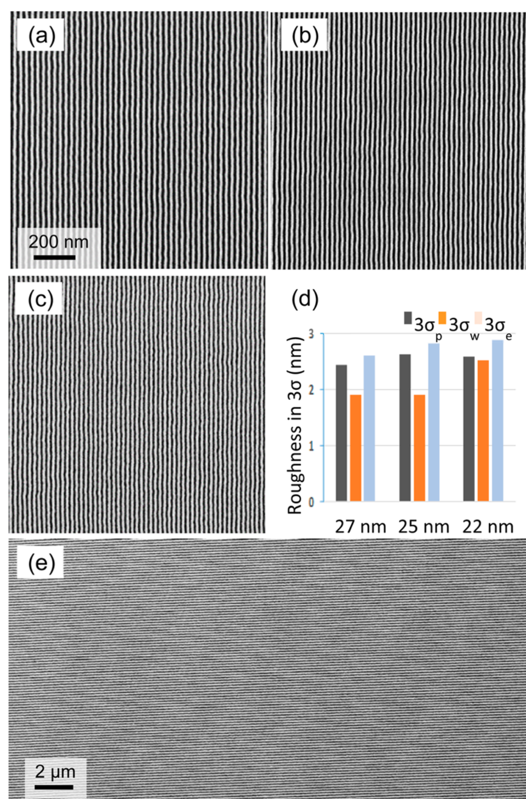

Figure 2. (a–c) Top-down SEM images of Si lines with full pitch of 27, 25, and 22 nm, respectively. The Si lines were fabricated using the process described in Figure 1. (d) Roughness data of Si lines. (e) Moiré SEM image of Si lines with 22 nm full pitch.

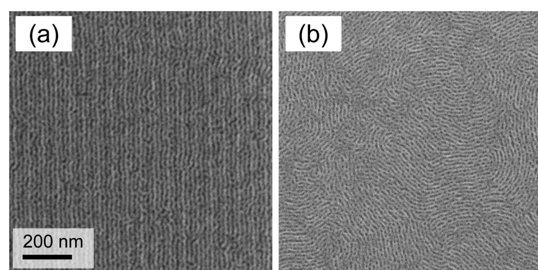

Figure 3. (a) Top-down SEM image of self-assembled lamellae-forming PS-*b*-PMMA with L_0 = 18.5 nm on a chemical pattern with L_s = 56 nm, w ∼ 0.6 L_0. (b) Fingerprint pattern of the BCP after O_2 plasma etching.

value of the PS-*b*-PMMA with L_0 of 22 nm is reduced to ∼15,[38] near the order−disorder transition point. Second, generating a chemical pattern suitable for a BCP with such small L_0 is near the limits of current lithography and etching tools (*e.g.*, e-beam writing of stripes with a period less than 45 nm using a positive-tone resist results in high roughness, and the roughness increases significantly when the stripes are trimmed to less than 15 nm in width). Third, any impurities in the BCPs, mats, and brushes may also induce roughness and defects. Long range ordering and registration in a large area are shown by a moiré interference pattern of the Si lines with full pitch of 22 nm (Figure 2e). Unlike the extremely strict requirement on defectivity demanded by semiconductor applications, BPM can tolerate more defects thanks to error correction codes used in HDDs. Therefore, our patterns can be successfully used for BPM, even though our fabrication standards in terms of environmental control and material purity are well below those found in semiconductor facilities. It is thus natural that our current defect densities are higher than the best reported by the semiconductor industry.[39,40] We estimate defect density by manually counting defects on SEM images taken at random locations on the wafer. Self-assembled BCP patterns are imaged after PMMA removal. On one wafer containing BCP patterns with L_0 of 25 nm, we took over 100 SEM images and found only one foreign particle on an area of ∼1700 μm^2. On another similar wafer, no defect was found in over 150 SEM images spanning a total area of ∼3400 μm^2. We found that the main contribution to the formation of defects comes from the pattern transfer step. After Cr/SOG pattern transfer, approximately one defect can be found in an area of ∼25 μm^2. This defect density is low enough for BPM applications, which require less than 1 defect in 1000 bits in the final magnetic disk.

We further explored the DSA of a PS-*b*-PMMA BCP with L_0 of 18.5 nm, close to the smallest period that can be obtained from a lamellae-forming PS-*b*-PMMA. The top-down SEM image of the BCP pattern self-assembled on one chemical pattern with $L_s \sim 3L_0$ and $w \sim 0.6L_0$ is shown on Figure 3a. Long range ordered DSA can be achieved but there are some dislocation defects. While DSA perfection might be achieved by refining the chemical patterns, the weak phase separation appears to be an insurmountable challenge for lithographic applications. As shown in Figure 3b, after O_2 RIE of the fingerprint patterns, there is no clear separation between PS and PMMA domains, which prevents subsequent pattern transfer with acceptable image quality. While the width of the interface Δ may have a dependence on pitch or degree of polymerization, it has been shown experimentally that for PS-*b*-PMMA $\Delta \approx 5$ nm independent of molecular weight.[32] For materials with a domain width below 10 nm, the interface width represents more than half the critical dimension. We attribute the observed difficulty in removing the PMMA domain cleanly to the large ratio of Δ/CD.

In comparison to conventional lithographic methods, one obvious limitation in BCP lithography lies in its restricted set of geometries. Forming arbitrary nonregular patterns, such as servo patterns, is challenging for BCP lithography. When topographic guiding patterns are used, servo patterns can be directly written as trenches by e-beam and then filled with BCP.[41,42] When chemical guiding patterns are used, the BCP must be coerced into forming servo patterns. If particularly complex servo patterns are required, BCPs cannot form the necessary patterns, and servo patterns have to be integrated by applying an additional lithographic step without DSA. However, we have proposed two relatively simple types of servo patterns—offset burst[43] and chevron[44] patterns—which can be generated by BCPs to encode the position information needed for track following. Offset burst patterns are a series of sections of circumferential lines that shift a fraction of a track along the cross track direction. Chevron patterns are sets of stripes in "Λ" shape. As shown in Figure 4a and b, a rotary stage e-beam system was used to first generate sparse chemical patterns containing offset burst and chevron patterns, respectively. The e-beam periods (line-to-line distance) of both offset burst and chevron patterns were set to be the same as those of the e-beam circumferential lines for the main data track patterns ($2L_0$). Self-assembly of a lamellae-forming PS-*b*-PMMA with L_0 of 27 nm was then carried out on the chemical patterns to double the density. The BCP patterns were then transferred to silicon substrate using the Cr/SOG process (Figure 4c and d). The offset burst patterns are readily revealed by a moiré SEM image (bottom in Figure 4a). A zoomed-in SEM image (top right in Figure 4a) shows that the left part of the parallel lines are shifted in steps of 6.25 nm ($0.25L_0$) in the direction normal to the circumferential lines. These offset features were duplicated on the final template after DSA and pattern transfer (Figure 4c). We also investigated DSA on offset burst patterns with different shifts. A series of offset patterns with L_s of 54 nm were written by rotary e-beam, with shifts from

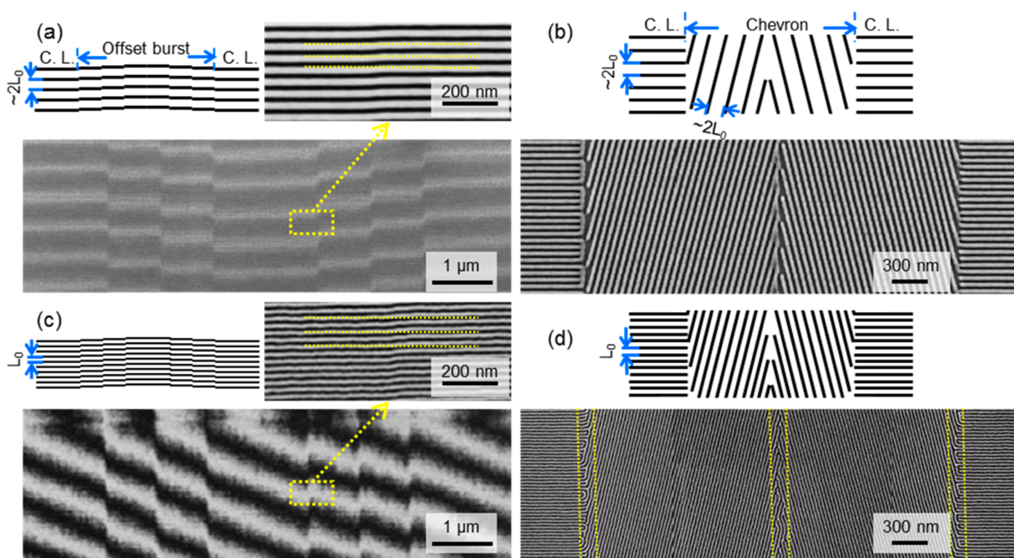

Figure 4. Schematic of BCP lithography on offset burst and chevron patterns. (a) Moiré and zoom-in SEM image of e-beam resist patterns containing both circumferential lines (C. L.) and offset bursts. (b) top-down SEM image of e-beam resist patterns containing both circumferential lines and chevrons. The periods (line-to-line distance) of circumferential lines, offset burst and chevron patterns equal to 2 L_0. DSA and subsequent pattern transfer were carried out to obtain Si lines with line-frequency doubled but retaining the same offset burst (c) or chevron features (d).

6 to 32 nm (Figure S2a). Self-assembled BCP patterns follow the offset patterns except at the boundaries where shifting occurs (Figure S2b). Although the e-beam written resist patterns have sharp offset shifts, gradual shifts are observed on the BCP patterns. From a thermodynamic standpoint, a sharp offset shift in BCP patterns is energetically unfavorable. Therefore, the shifts occur in a gradual manner, and a larger shift in BCP patterns always results in a larger transition region. Formation of servo patterns by DSA on chevron patterns with density multiplication has also been reported by our group.[44] In that work, guiding patterns were written by an $x-y$ stage e-beam lithography system. Similar to those results, we found DSA defects at chevron apexes as well as the junction between the circumferential lines and chevrons. The widths of those defective areas, highlighted by the yellow dotted lines, are less than 150 nm. These defects originate from the incapability of BCP lamellae to bend at sharp angles, and also defects in the guiding patterns originating in the e-beam system. Except in these interfacial areas, chevron patterns are parallel lines with L_s commensurate to L_0. Away from the apex area, the DSA quality should be independent of the chevron angles. However, we observed defective DSA when the chevron angle is greater than 40°, which is caused by the degradation of resist pattern quality (Figure S3).

According to the proposed process for high volume manufacturing of BPM,[45,46] our goal is to fabricate imprintable master templates with islands over a full-disk area. Since we aim to generate master templates containing rectangular islands in a locally quasi-rectangular lattice (actually in circular tracks at the macro scale) using a double imprint process, two submaster templates with full-disk area are required.[24] As a demonstration, we fabricated one submaster template with 24.5 nm circumferential lines on a full annular band between radii of 13 and 38 mm, which is more than what is needed to fill a 2.5 inch magnetic recording disk. For fabrication of templates with such large area, the low throughput of e-beam writing is one of the main hurdles. Decreasing e-beam dosage is one direct method to improve the throughput; however, it would degrade the e-beam resist pattern quality. Typically, we expose ZEP resist at a dose of ~89 fC/μm and develop in ZED-N50 at 2 °C for 17 s to obtain line patterns with full pitch down to 35 nm. If the dose is halved, (resist is developed in ZED-N50 at 20 °C for 60 s), the line roughness will increase and the resist resolution will decrease. Using low e-beam dose, we are still able to obtain line patterns with a full pitch above 44 nm, on which a nearly perfect DSA can occur (Figure S4). For the template with a 25 mm wide band, using a low e-beam dose (~46 fC/μm), it took more than 10 days to write circumferential lines with L_s of 49 nm. It would take more than 17 days if a dose of ~89 fC/μm were used. Across the band, the e-beam resist patterns show similar quality (Figure S5), which indicates stable e-beam writing conditions. DSA and pattern transfer were then carried out using the procedures described earlier. The uniformity of the resist pattern helped in achieving perfect DSA over the whole area (Figure S6). After pattern transfer into the Si substrate, the template was imaged by SEM revealing Si lines with similar quality at different radii and random azimuthal locations (Figure 5a). In terms of roughness ($3\sigma_e$ = 2.58 nm, $3\sigma_w$ = 1.95 nm, and $3\sigma_p$ = 2.39 nm), the Si lines on this template are similar to those on wafers with smaller

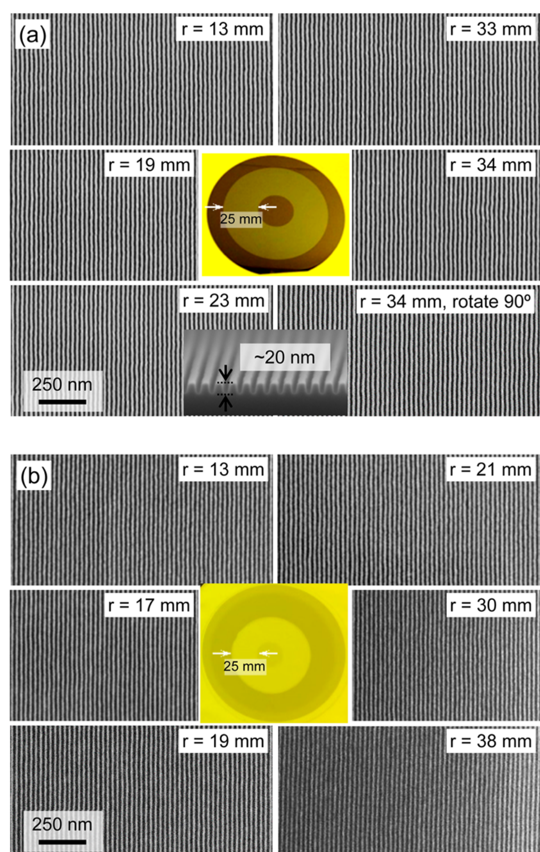

Figure 5. (a) Top-down SEM images of one template containing circumferential lines with 24.5 nm in full pitch on 25 mm-wide full band circular tracks. The images were taken at different radii. The middle shows one photo of the template containing e-beam resist pattern of 49 nm circumferential lines. Inset: cross section SEM image of Si lines on a sister sample. (b) Top-down SEM images of resist patterns imprinted from the template shown above. The images were taken at different radii. The middle shows one photo of one imprinted quartz wafer.

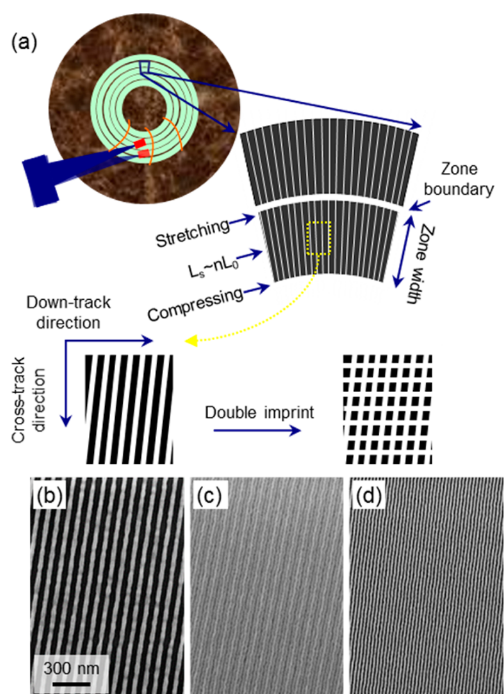

Figure 6. (a) Schematic representation of zoning and skew. (b−d) Top-down SEM images of a template with skewed radial lines at different stages: (b) e-beam resist pattern with $L_s \sim 3L_0$, (c) self-assembled BCP pattern with period $\sim L_0$, and (d) Si lines.

area patterns. The height of the Si lines is approximately 20 nm as shown in the inset cross-sectional SEM image of a sister sample. Furthermore, we used this template to imprint on a transparent quartz substrate. The imprint resist patterns were imaged by SEM after being coated by a thin layer of Cr for conductivity (Figure 5b). The results confirmed uniform and high-fidelity imprinting across the band. The roughness data of the imprint resist pattern are as follows: $3\sigma_e$ = 2.37 nm, $3\sigma_w$ = 2.39 nm, and $3\sigma_p$ = 2.02 nm. These values are slightly different than those of the Si lines. First, the Si lines show a low width roughness inherited from the excellent width uniformity typical of BCP self-assembly. On the other hand, imprint resist lines show a better edge roughness, which may be due to shrinking of the resist during curing.

In addition to submaster templates with circumferential lines, we also fabricated submaster templates with radial lines of constant angular pitch. In order to fabricate templates with areal density greater than 1.2 Tdot/in^2 at our target BAR, a full pitch less than 20.5 nm is required for the radial lines, which is beyond the limits of PS-*b*-PMMA pattern transfer. Therefore, we either need to introduce another BCP material with higher χ value, or to combine a line-frequency doubling process[26] with our current BCP lithography. Much effort has been made on both approaches. Here, generating radial lines from PS-*b*-PMMA has two purposes: one is to fabricate templates with an areal density lower than 1.2 Tdot/in^2, another is to generate mandrel line patterns for the line frequency doubling process for higher density templates. The radial lines are typically divided into zones (as shown in Figure 6a), and the angular pitch is only kept constant within each zone. In this way, we can obtain dense radial lines over the whole disk area, and achieve high areal density in all regions of the final template. Within a zone, we generally set the lateral period of the radial lines equal to L_0 in the middle of the zone, with the BCP lamellae compressing and stretching along the cross track (radial) direction toward the inner and outer diameters of the disk, respectively. For a zone width of 0.5 mm, the BCP lamellae have to compress and stretch ~2%, which can be readily achieved (Figure S7). Skewing is also required for the radial lines due to the current mechanical design of HDDs (as shown in Figure 6a). Here, skewed radial lines can be naturally formed by the rotary stage e-beam tool (Figure 6b). DSA of a lamellae-forming PS-*b*-PMMA with L_0 of 25 nm was then carried out to multiply the density of the e-beam resist pattern by 3X while retaining the same skew angle (Figure 6c). The BCP patterns were then transferred to the Si substrate (Figure 6d). It is noteworthy to

consider that in the originally proposed geometry for BPM comprising round dots in a hexagonal lattice,[2−4,6] and assuming that the increased track density requires a hyper-track configuration to accommodate for the relatively wide head,[47,48] it would be extremely challenging to achieve the desired skew angle of ±15°. Local stretching and/or compressing of BCP morphologies is required to form skewed hexagonal patterns, and more stretching and/or compressing is needed for a higher skew angle. The maximum achievable skew angles are determined by whether the stretching and/or compressing can be tolerated by the BCP pattern. Previous studies show that the maximum achievable skew angles are ~7° and ~8° for cylinder-forming PS-*b*-PMMA[4] and sphere-forming PS-*b*-PDMS,[49] respectively. In comparison to skewed hexagonal patterns, skewed radial line patterns are parallel lines with constant spacing, and don not involve any pitch variation. Therefore, BCP patterns can follow radial lines with arbitrary skew angle.

CONCLUSION

In summary, we explored the limits of lamellae-forming PS-*b*-PMMA for lithographic applications by conducting DSA on chemical patterns using a LINE flow and pattern transfer to Si substrate using a Cr/SOG process. Our results show that nearly perfect DSA may be obtained as long as the BCP can phase separate (L_0 = 18.5 nm); however, high-fidelity pattern transfer can only be achieved at a larger pitch (L_0 ~22 nm). The main challenge is the formation of a well-defined mask after PMMA removal. Creating a sharp, well-defined mask depends on both the ability to cleanly and selectively remove one block and on the ratio of Δ/CD. In this work, we were able to successfully demonstrate pattern transfer when Δ/CD is less than 0.5. BCP lithography using lamellae-forming PS-*b*-PMMA was further investigated with the view of fabricating nanoimprint templates for BPM applications. We studied the pattern quality in terms of defectivity and line roughness; we demonstrated compatibility with hard disk drive architecture by fabricating skewed radial lines with constant angular pitch, and circumferential lines alternating with offset burst or chevron patterns; and nanoimprint template fabrication and nanoimprinting were demonstrated on full annular bands of circular tracks up to 25 mm wide.

METHODS

PS-*b*-PMMA (M_n = 25−26 kg/mol, polydispersity index (PDI) = 1.06) was purchased from Polymer Source Inc. and was dissolved in toluene with a concentration of 1.5 wt %. PS-*b*-PMMAs with L_0 of 25, 22, 18.5 nm, the cross-linkable polystyrene, and hydroxyl terminated poly(styrene-*ran*-methyl methacrylate) (PS-*r*-PMMA-OH) were received as solutions in propylene glycol methyl ether acetate (PGMEA) from EMD Performance Materials Corp. ZEP520A e-beam resist and developer ZED-N50 were from Zeon Corp. SOG solution was from Futurrex Inc.

Experimental results in this study were conducted on full 100 mm double side polished Si wafers. The cross-linkable PS solution was spin-coated on silicon wafers and annealed at 250 °C for 2 h under vacuum, resulting in a cross-linked PS (XPS) layer with thickness of ~7−8 nm. A 50 nm-thick ZEP520A e-beam resist film was deposited onto the silicon substrates grafted with XPS and baked at 170 °C for 5 min. The resist patterns were exposed by a rotary stage e-beam lithography system (Elionix EBW7000C) with an acceleration voltage of 100 kV. The exposed resist patterns were developed with ZED-N50 and rinsed with IPA. The resist patterns were trimmed to target width and transferred to the XPS layer by a timed 10 W O_2 RIE for 70−200 s. After removal of the resist with NMP, a 20 nm-thick film of PS-*r*-PMMA-OH with 50 mol % of styrene content was spin-coated onto the patterned substrate. The substrate was then annealed at 200 °C for 30 min to graft the brush into the regions between the XPS stripes. Excess PS-*r*-PMMA-OH was removed by sonication in NMP to yield chemical patterns of alternating XPS stripes and PS-*r*-PMMA stripes. PS-*b*-PMMA BCPs were coated on the chemical patterns and annealed at 250 °C for 5 to 60 min. The BCP film thickness was ~1−1.5 L_0. After forming the DSA patterns, the PMMA block was selectively removed by an anisotropic O_2 RIE process (60 W, 2 mTorr, 20−25 s). Then a thin layer of Cr (~3−5 nm in thickness) was deposited on the remaining PS lines from a normal incidence by e-beam evaporation. The patterns were then planarized by spin-coating a SOG layer. CHF_3/O_2 RIE (15 W, 3.5 mTorr, 6−10 s) was then carried out to etch back the SOG in order to reveal the Cr layer above the PS lines. Cl_2/O_2 (20 W, 10 mTorr, 15 s) and O_2 RIE (60 W, 2 mTorr, 10−25 s) were subsequently used to etch the revealed Cr layer on top of the PS lines and the PS lines, respectively. $CF_4/CHF_3/Ar$ RIE (30 W, 2.5 mTorr, 20−30 s) was used to transfer the Cr lines into the Si substrate. The remaining Cr was removed in a Cr etchant (CR9S). A UV cure ink jet dispense nanoimprinting process[50] was conducted to transfer the patterns on Si substrate to a quartz substrate. The imprint tool is an Imprio 1100 single side imprinter from Molecular Imprints Inc. A Zeiss Ultra55 field-emmisson SEM was used to image the samples using 1 or 5 kV acceleration voltage.

Conflict of Interest: The authors declare no competing financial interest.

Supporting Information Available: Figures containing more experimental results. The Supporting Information is available free of charge on the ACS Publications website at DOI: 10.1021/acsnano.5b02613.

REFERENCES AND NOTES

1. International Technology Roadmap for Semiconductors. http://www.itrs.net/home.html, accessed May 2015.
2. Ross, C. A.; Cheng, J. Y. Patterned Magnetic Media Made by Self-Assembled Block-Copolymer Lithography. *MRS Bull.* **2008**, *33*, 838–845.
3. Ruiz, R.; Kang, H. M.; Detcheverry, F. A.; Dobisz, E.; Kercher, D. S.; Albrecht, T. R.; de Pablo, J. J.; Nealey, P. F. Density Multiplication and Improved Lithography by Directed Block Copolymer Assembly. *Science* **2008**, *321*, 936–939.
4. Yang, X.; Wan, L.; Xiao, S.; Xu, Y.; Weller, D. Directed Block Copolymer Assembly *Versus* Electron Beam Lithography for Bit Patterned Media with Areal Density of 1 Terabit/inch^2 and Beyond. *ACS Nano* **2009**, *3*, 1844–1858.
5. Xiao, S.; Yang, X.; Park, S.; Weller, D.; Russell, T. P. A General Approach to Addressable 4 Tdot/in^2 Pattered Media. *Adv. Mater.* **2009**, *21*, 2516–2519.
6. Naito, K.; Hieda, H.; Sakurai, M.; Kamata, Y.; Asakawa, K. 2.5-Inch Disk Patterned Media Prepared by an Artificially

Assisted Self-Assembling Method. *IEEE Trans. Magn.* **2002**, *38*, 1949–1951.

7. Kim, S. O.; Solak, H. H.; Stoykovich, M. P.; Ferrier, N. J.; de Pablo, J. J.; Nealey, P. F. Epitaxial Self-Assembly of Block Copolymers on Lithographically Defined Nanopatterned Substrates. *Nature* **2003**, *424*, 411–414.
8. Stoykovich, M. P.; Muller, M.; Kim, S. O.; Solak, H. H.; Edwards, E. W.; de Pablo, J. J.; Nealey, P. F. Directed Assembly of Block Copolymer Blends into Nonregular Device-Oriented Structures. *Science* **2005**, *308*, 1442–1446.
9. Cheng, J. Y.; Rettner, C. T.; Sanders, D. P.; Kim, H. C.; Hinsberg, W. D. Dense Self-Assembly on Sparse Chemical Patterns: Rectifying and Multiplying Lithographic Patterns Using Block Copolymers. *Adv. Mater.* **2008**, *20*, 3155–3158.
10. Liu, C. C.; Ramirez-Hernandez, A.; Han, E.; Craig, G. S. W.; Tada, Y.; Yoshida, H.; Kang, H. M.; Ji, S. X.; Gopalan, P.; de Pablo, J. J.; Nealey, P. F. Chemical Patterns for Directed Self-Assembly of Lamellae-Forming Block Copolymers with Density Multiplication of Features. *Macromolecules* **2013**, *46*, 1415–1424.
11. Rockford, L.; Liu, Y.; Mansky, P.; Russell, T. P.; Yoon, M.; Mochrie, S. G. J. Polymers on Nanoperiodic, Heterogeneous Surfaces. *Phys. Rev. Lett.* **1999**, *82*, 2602.
12. Yang, X.; Xiao, S.; Hsu, Y.; Feldbaum, M.; Lee, K.; Kuo, D. Directed Self-Assembly of Block Copolymer for Bit Patterned Media with Areal Density of 1.5 Teradot/Inch^2 and Beyond. *J. Nanomater.* **2013**, *2013*, 17.
13. Segalman, R. A.; Yokoyama, H.; Kramer, E. J. Graphoepitaxy of Spherical Domain Block Copolymer Films. *Adv. Mater.* **2001**, *13*, 1152.
14. Cheng, J. Y.; Ross, C. A.; Thomas, E. L.; Smith, H. I.; Vancso, G. J. Fabrication of Nanostructures with Long-Range Order Using Block Copolymer Lithography. *Appl. Phys. Lett.* **2002**, *81*, 3657–3659.
15. Cheng, J. Y.; Mayes, A. M.; Ross, C. A. Nanostructure Engineering by Templated Self-Assembly of Block Copolymers. *Nat. Mater.* **2004**, *3*, 823–828.
16. Xiao, S. G.; Yang, X. M.; Edwards, E. W.; La, Y. H.; Nealey, P. F. Graphoepitaxy of Cylinder-Forming Block Copolymers for Use as Templates to Pattern Magnetic Metal Dot Arrays. *Nanotechnology* **2005**, *16*, S324–S329.
17. Park, S.-M.; Liang, X.; Harteneck, B. D.; Pick, T. E.; Hiroshiba, N.; Wu, Y.; Helms, B. A.; Olynick, D. L. Sub-10 nm Nanofabrication *via* Nanoimprint Directed Self-Assembly of Block Copolymers. *ACS Nano* **2011**, *5*, 8523–8531.
18. Mansky, P.; Liu, Y.; Huang, E.; Russell, T. P.; Hawker, C. J. Controlling Polymer-Surface Interactions with Random Copolymer Brushes. *Science* **1997**, *275*, 1458–1460.
19. Ryu, D. Y.; Shin, K.; Drockenmuller, E.; Hawker, C. J.; Russell, T. P. A Generalized Approach to the Modification of Solid Surfaces. *Science* **2005**, *308*, 236–239.
20. Han, E.; In, I.; Park, S. M.; La, Y. H.; Wang, Y.; Nealey, P. F.; Gopalan, P. Photopatternable Imaging Layers for Controlling Block Copolymer Microdomain Orientation. *Adv. Mater.* **2007**, *19*, 4448–4452.
21. Bates, F. S.; Fredrickson, G. H. Block Copolymer Thermodynamics: Theory and Experiment. *Annu. Rev. Phys. Chem.* **1990**, *41*, 525–557.
22. Anastasiadis, S. H.; Russell, T. P.; Satija, S. K.; Majkrzak, C. F. Neutron Reflectivity Studies of the Surface-Induced Ordering of Diblock Copolymer Films. *Phys. Rev. Lett.* **1989**, *62*, 1852–1855.
23. Ruiz, R.; Dobisz, E.; Albrecht, T. R. Rectangular Patterns Using Block Copolymer Directed Assembly for High Bit Aspect Ratio Patterned Media. *ACS Nano* **2011**, *5*, 79–84.
24. Wan, L.; Ruiz, R.; Gao, H.; Patel, K. C.; Lille, J.; Zeltzer, G.; Dobisz, E. A.; Bogdanov, A.; Nealey, P. F.; Albrecht, T. R. Fabrication of Templates with Rectangular Bits on Circular Tracks by Combining Block Copolymer Directed Self-Assembly and Nanoimprint Lithography. *J. Micro/Nanolithogr., MEMS, MOEMS* **2012**, *11*, 0314051–0314055.
25. Albrecht, T. R.; Arora, H.; Ayanoor-Vitikkate, V.; Beaujour, J.; Bedau, D.; Berman, D.; Bogdanov, A. L.; Chapuis, Y.; Cushen, J.; Dobisz, E. E.; *et al.* Bit-Patterned Magnetic Recording: Theory, Media Fabrication, and Recording Performance. *IEEE Trans. Magn.* **2015**, *51*, 1–42.
26. Patel, K. C.; Ruiz, R.; Lille, J.; Wan, L.; Dobisz, E. A.; Gao, H.; Albrecht, T. R.; Robertson, N. Line-Frequency Doubling of Directed Self-Assembly Patterns for Single-Digit Bit Pattern Media Lithography. *Proc. SPIE* **2012**, *8323*, 83230U.
27. Liu, C. C.; Han, E.; Onses, M. S.; Thode, C. J.; Ji, S. X.; Gopalan, P.; Nealey, P. F. Fabrication of Lithographically Defined Chemically Patterned Polymer Brushes and Mats. *Macromolecules* **2011**, *44*, 1876–1885.
28. Leibler, L. Theory of Microphase Separation in Block Copolymers. *Macromolecules* **1980**, *13*, 1602–1617.
29. Walton, D. G.; Kellogg, G. J.; Mayes, A. M.; Lambooy, P.; Russell, T. P. A Free-Energy Model for Confined Diblock Copolymers. *Macromolecules* **1994**, *27*, 6225–6228.
30. Helfand, E.; Tagami, Y. Theory of the Interface between Immiscible Polymers. *J. Polym. Sci., Part B: Polym. Lett.* **1971**, *9*, 741–746.
31. Hadjichristidis, N.; Pispas, S.; Floudas, G. *Block Copolymers: Synthetic Strategies, Physical Properties, and Applications*; John Wiley & Sons Inc.: Hoboken, NJ, 2003.
32. Sunday, D. F.; Ashley, E.; Wan, L.; Patel, K. C.; Ruiz, R.; Kline, R. J. Template−Polymer Commensurability and Directed Self-Assembly Block Copolymer Lithography. *J. Polym. Sci., Part B: Polym. Phys.* **2015**, *53*, 595–603.
33. Chevalier, X.; Nicolet, C.; Tiron, R.; Gharbi, A.; Argoud, M.; Pradelles, J.; Delalande, M.; Cunge, G.; Fleury, G.; Hadziioannou, G.; Navarro, C. Scaling-Down Lithographic Dimensions with Block-Copolymer Materials: 10-nm-Sized Features with Poly(styrene)-*block*-poly(methylmethacrylate). *J. Micro/Nanolithogr., MEMS, MOEMS* **2013**, *12*, 031102.
34. Tsai, H.; Pitera, J. W.; Miyazoe, H.; Bangsaruntip, S.; Engelmann, S. U.; Liu, C.-C.; Cheng, J. Y.; Bucchignano, J. J.; Klaus, D. P.; Joseph, E. A.; *et al.* Two-Dimensional Pattern Formation Using Graphoepitaxy of PS-*b*-PMMA Block Copolymers for Advanced FinFET Device and Circuit Fabrication. *ACS Nano* **2014**, *8*, 5227–5232.
35. Rathsack, B.; Somervell, M.; Hooge, J.; Muramatsu, M.; Tanouchi, K.; Kitano, T.; Nishimura, E.; Yatsuda, K.; Nagahara, S.; Hiroyuki, I.; *et al.* Pattern Scaling with Directed Self Assembly Through Lithography and Etch Process Integration. *Proc. SPIE* **2012**, *8323*, 83230B.
36. Tsai, H. Y.; Miyazoe, H.; Engelmann, S.; To, B.; Sikorski, E.; Bucchignano, J.; Klaus, D.; Liu, C. C.; Cheng, J.; Sanders, D.; Fuller, N.; Guillorn, M. Sub-30nm Pitch Line-Space Patterning of Semiconductor and Dielectric Materials Using Directed Self-Assembly. *J. Vac. Sci. Technol. B* **2012**, *30*, 6.
37. Tsai, H.; Miyazoe, H.; Cheng, J.; Brink, M.; Dawes, S.; Klaus, D.; Bucchignano, J.; Sanders, D.; Joseph, E.; Colburn, M.; Guillorn, M. A. Self-Aligned Line-Space Pattern Customization with Directed Self-Assembly Grapho-Epitaxy at 24nm Pitch. *Proc. SPIE* **2015**, *9423*, 942314.
38. Sivaniah, E.; Matsubara, S.; Zhao, Y.; Hashimoto, T.; Fukunaga, K.; Kramer, E. J.; Mates, T. E. Symmetric Diblock Copolymer Thin Films on Rough Substrates: Microdomain Periodicity in Pure and Blended Films. *Macromolecules* **2008**, *41*, 2584–2592.
39. Bencher, C.; Smith, J.; Miao, L.; Cai, C.; Chen, Y.; Cheng, J. Y.; Sanders, D. P.; Tjio, M.; Truong, H. D.; Holmes, S.; Hinsberg, W. D. Self-Assembly Patterning for Sub-15nm Half-Pitch: A Transition from Lab to Fab. *Proc. SPIE* **2011**, *7970*, 79700F.
40. Rincon Delgadillo, P.; Harukawa, R.; Suri, M.; Durant, S.; Cross, A. Defect Source Analysis of Directed Self-Assembly Process (DSA of DSA). *Proc. SPIE* **2013**, *8680*, 86800L.
41. Yamamoto, R.; Yuzawa, A.; Shimada, T.; Ootera, Y.; Kamata, Y.; Kihara, N.; Kikitsu, A. Nanoimprint Mold for 2.5 Tbit/in.^{2} Directed Self-Assembly Bit Patterned Media with Phase Servo Pattern. *Jpn. J. Appl. Phys.* **2012**, *51*, 046503.
42. Yang, X.; Xiao, S.; Hsu, Y.; Wang, H.; Hwu, J.; Steiner, P.; Wago, K.; Lee, K.; Kuo, D. Fabrication of Servo-Integrated Template for 1.5 Teradot/inch^2 Bit Patterned Media with Block Copolymer Directed Assembly. *J. Micro/Nanolithogr., MEMS, MOEMS* **2014**, *13*, 031307.
43. Lille, J.; Ruiz, R.; Wan, L.; Gao, H.; Dhanda, A.; Zeltzer, G.; Arnoldussen, T.; Patel, K.; Tang, Y.; Kercher, D.; Albrecht, T. R.

Integration of Servo and High Bit Aspect Ratio Data Patterns on Nanoimprint Templates for Patterned Media. *IEEE Trans. Magn.* **2012**, *48*, 2757–2760.
44. Liu, G.; Nealey, P. F.; Ruiz, R.; Dobisz, E.; Patel, K. C.; Albrecht, T. R. Fabrication of Chevron Patterns for Patterned Media with Block Copolymer Directed Assembly. *J. Vac. Sci. Technol., B* **2011**, *29*, 06F204.
45. Terris, B.; Thomson, T.; Hu, G. Patterned Media for Future Magnetic Data Storage. *Microsyst. Technol.* **2007**, *13*, 189–196.
46. Albrecht, T. R.; Hellwing, O.; Ruiz, R.; Schabes, M. E.; Terris, B. D.; Wu, X. Z. Bit-Patterned Magnetic Recording: Nanoscale Magnetic Islands for Data Storage. In *Nanoscale Magnetic Materials and Applications*; Liu, J. P., Fullerton, E., Gutfleisch, O., Sellmyer, D. J., Eds.; Springer: New York, 2009; pp 237−274.
47. Rubin, K. A.; Terris, B. D. Patterned Media Having Offset Tracks. U. S. Patent 10/042,132, Aug. 30, 2005.
48. Richter, H.; Dobin, A.; Weller, D. Data Storage Device with Bit Patterned Media with Staggered Islands. U. S. Patent 11/430,809, Nov 8, 2007.
49. Xiao, S.; Yang, X.; Lee, K. Y.; Hwu, J. J.; Wago, K.; Kuo, D. Directed Self-Assembly for High-Density Bit-Patterned Media Fabrication Using Spherical Block Copolymers. *J. Micro/Nanolithogr., MEMS, MOEMS* **2013**, *12*, 031110.
50. Resnick, D. J.; Sreenivasan, S. V.; Willson, C. G. Step & Flash Imprint Lithography. *Mater. Today* **2005**, *8*, 34–42.